Journal of Power Sources 216 (2012) 5–10

Contents lists available at SciVerse ScienceDirect

Journal of Power Sources

journal homepage: www.elsevier.com/locate/jpowsour

Short communication

Study of a graphene-like anode material in *N*-methyl-*N*-propylpyrrolidinium bis(trifluoromethanesulfonyl)imide ionic liquid for Li-ion batteries

Maciej Galinski, Ilona Acznik*

Faculty of Chemical Technology, Poznan University of Technology, 60 965 Poznan, Poland

HIGHLIGHTS

- Presented work concerns graphene-like material as an anode in lithium-ion cell.
- Conventional electrolyte was replaced by ionic liquid.
- Satisfactory capacity of the material working with ionic liquid was obtained.
- Mechanism of Li storage in these materials is determined to be quite complex.
- No well-defined charging/discharging plateau was recorded.

ARTICLE INFO

Article history:
Received 28 February 2012
Received in revised form
8 May 2012
Accepted 16 May 2012
Available online 23 May 2012

Keywords:
Graphite oxide
Graphene sheets
Ionic liquids
Lithium-ion batteries

ABSTRACT

Graphene nanosheets or reduced graphite oxide materials recently have attracted great attention because of their excellent electrochemical properties such as excellent electrical conductivity and high specific capacity originating from their structure, i.e., two-dimensional layers with one-atomic thickness. This work is focused on reduced graphite oxide (RGO) applied as negative electrode in Li-ion cell with ionic liquid (*N*-methyl-*N*-propylpyrrolidinium bis(trifluoromethanesulfonyl)imide, Py13TFSI) as electrolyte. Three different electrochemical techniques, e.g., galvanostatic charging/discharging, cyclic voltammetry and electrochemical impedance spectroscopy were applied for full electrochemical characterisation of these materials. The results proved that RGO gives good reversible capacity of ca. 550 mAh g^{-1} (at current density of 50 mA g^{-1}) working together with the ionic liquid. This value is comparable to that characteristic for cells operating with conventional electrolyte (cyclic carbonates).

1. Introduction

The appearance of portable devices on the market led to increase of the interest in electrochemical power sources. Well-known and currently intensively investigated energy storage devices are lithium-ion batteries [1,2]. They have revolutionized portable electronic devices, becoming the main source of energy for mobile phones, cameras, laptops, etc. Moreover, they are the most promising option for the supply of hybrid vehicles (HEVs) or electric vehicles (EVs) [3]. To improve their electrochemical properties, the main attention is focused on the design of electrode materials [4,5]. Additionally, they must be safe for users and environmentally friendly. Implementation of large-scale lithium cells is restricted by currently used electrolyte (liquid organic carbonates). The replacement of the conventional, flammable and volatile organic solutions with ionic liquid-based electrolytes might greatly reduce the risk of thermal runaway. This provides the lithium battery level of safety required for their large-scale application in important and strategic markets, e.g., the automotive industry where they serve as a power source in hybrid or hybrid electric vehicles [6].

Li-ion battery anodes generally are prepared of graphite with a theoretical capacity of 372 mAh g^{-1}. Presently, an improved form of graphite, graphene nanosheets (GNSs) occupy a large part of the researches presented in the literature [7–10]. The way to obtain this kind of material occurs in two main steps. The first stage involves the oxidation process resulting in a graphite oxide (GO), which must be reduced chemically, thermally or electrochemically to unoxidized form in the next step [11–15]. Mechanical, electrochemical and thermal properties of the material depend on the method of preparation. Because of great GNSs advantages such as high surface area (theoretically over 2,600 m^2 g^{-1}), superior electrical conductivity, excellent thermal and mechanical properties, they were studied from the point of view of their application in capacitors and for hydrogen storage [16–18]. By increasing

* Corresponding author. Tel.: +48 61 665 23 10; fax: +48 61 665 25 71.
E-mail address: ilona.h.acznik@doctorate.put.poznan.pl (I. Acznik).

0378-7753/$ – see front matter © 2012 Elsevier B.V. All rights reserved.
doi:10.1016/j.jpowsour.2012.05.039

theoretical capacity to 744 mAh g^{-1} through the expansion of the interlayer space, GNSs also can be used in Li-ion batteries [19–23]. The mechanism of lithium storage can be explained in various ways. The irreversible insertion of lithium results in the formation of the solid electrolyte interface film (SEI) on the electrode surface, while defects on the edges and internal which do not have contact with the electrolyte contribute to the reversible storage [20].

In this work, graphene-like material (i.e., reduced graphite oxide, RGO) was obtained by thermal reduction followed by chemical oxidation of natural graphite and was then tested as a negative electrode in the lithium-ion cell with pyrrolidinium-based ionic liquid as the electrolyte.

2. Experimental

2.1. Synthesis of reduced graphite oxide

Graphite oxide (GO) was synthesized from natural graphite powder (SL-20, Superior Graphite, USA) by a modified Hummers method [24]. Briefly, 3.0 g of the graphite was added into 120 ml of concentrated H_2SO_4 (95–98%) and stirred for 24 h. Then, 2.5 g of $NaNO_3$ was added into the solution and after 2 h 15 g of $KMnO_4$ was also added under constant stirring. The temperature of the mixture was kept below 6 °C (ice bath). The reaction was continued for 3 h in the temperature range 2–3 °C and then 1 h at room temperature. After that the mixture was diluted with distilled water. Addition of water was performed in an ice bath to keep the temperature below 40 °C. After temperature stabilization (24–27 °C), 30% H_2O_2 was added to reduce the residual $KMnO_4$. During this reaction a large amount of bubbles was released and the colour of the mixture changed from brown-green to yellow. The general procedure for the oxidation of graphite is shown in Scheme 1. The as-obtained GO was filtered and washed with 35–38% HCl aqueous solution (1:10, 1,000 ml) followed by washing with distilled water. Finally, to remove residues of used salts and acids, obtained GO was re-dispersed in water and then dialyzed (dialysis sacks, pore size 12,000 Da, Sigma–Aldrich) to pH change from 2.6 to neutral. The resulting GO were dried at 65 °C in a vacuum.

Obtained GO was thermally reduced in a tube furnace in a helium (RGO-1) or hydrogen (RGO-2) atmosphere at 380 °C within 2 h with a heating rate of 5 °C min^{-1}.

2.2. Morphology and structure

The Raman scattering spectra were recorded in the range of 100 cm^{-1} - 3,400 cm^{-1}. The non-polarized Raman spectra were recorded in the back scattering geometry using inVia Renishaw micro-Raman system. The light blue line of argon laser operating at 488 nm was used. The inVia Raman spectrometer allowed to record the Raman spectra with the spatial resolution of about 1 μm. The spectral resolution was 2 cm^{-1}. The morphology of the prepared RGO was observed by scanning electron microscope (SEM, Tescan Vega 5153).

2.3. Electrode preparation and electrochemical measurements

Graphene-like materials obtained from thermal reduction were mixed with a binder poly(vinylidene fluoride) (PVdF, Fluka) and carbon black (CB, Alfa Aesar) at weight ratios of 70:20:10 in *N*-methyl-2-pyrrolidone (NMP, Fluka). Obtained slurry was coated on Cu-foil current collector (diameter 10 mm). The electrodes were dried in three steps: 24 h at room temperature, 24 h at 65 °C and 24 h at 120 °C in a vacuum drier.

0.7 M lithium bis(trifluoromethanesulfonyl)imide (LiTFSI, Fluka) in *N*-methyl-*N*-propylpyrrolidinium bis(trifluoromethanesulfonyl) imide (Py13TFSI) ionic liquid prepared as reported elsewhere [25] was used as the electrolyte. Vinylene carbonate (VC, Aldrich) was used as an additive, able to form SEI at the electrode/electrolyte interface. Lithium foil (0.75 mm thick, Aldrich) was used as the counter and reference electrode. Cells were assembled in a glove box in inert Ar atmosphere. Electrodes were separated by a glass micro-fibre GF/A separator (Whatman) and placed in an adopted 0.5″ Swagelok® connecting tube. Galvanostatic charging/discharging method was performed with the use of the ATLAS 0691 MBI multichannel electrochemical system (Atlas–Solich, Poland) at current density of 50 mA g^{-1} between 0.005 and 3 V versus the lithium-metal reference electrode. Impedance spectra were recorded using an ac impedance analyzer G™750 Potentiostat/Galvanostat/ZRA (Gamry Instruments, USA) in a frequency range of 100 kHz–10 mHz with potential amplitude 10 mV. Deconvolution of spectra was performed with the Z-view software (Scribner Associates Inc., USA). Cyclic voltammetry measurement were carried out in the potential range 0.005–3.0 V vs. Li/Li^+ with the

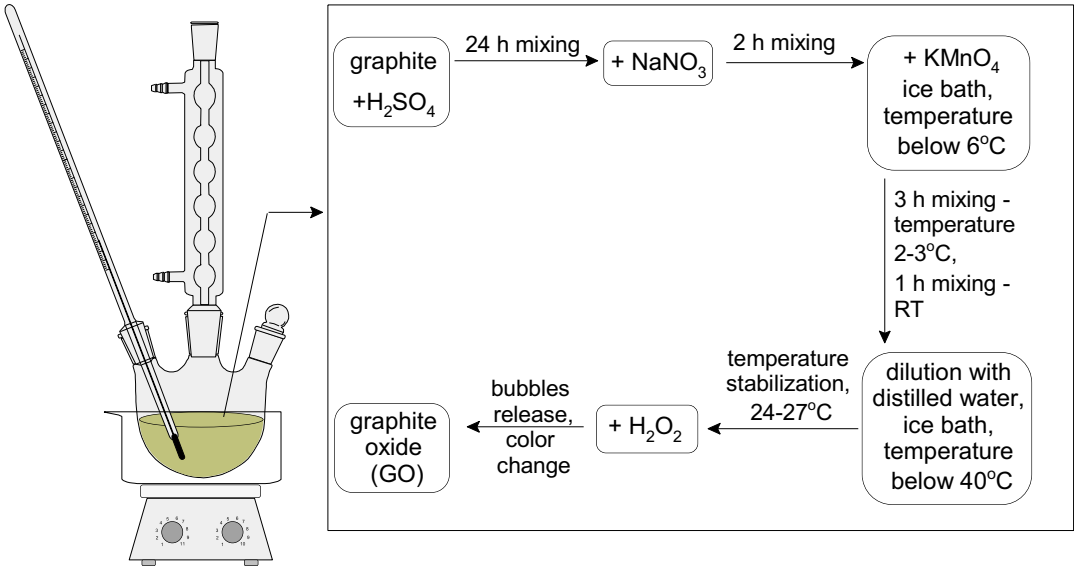

Scheme 1. Schematic illustration of procedure for the chemical process of oxidation of graphite.

scan rate of 0.1 mV s^{-1} using the μAutolab type II electrochemical system (Ecochemie, The Netherlands).

3. Results and discussion

The structural changes occurring during the chemical conversion of the graphite to graphite oxide and then to the reduced GO, were investigated by Raman spectroscopy, as shown in Fig. 1. For the natural graphite (Fig. 1a), the spectrum displays a G peak at 1,579 cm^{-1}, corresponding to the first-order scattering of the E_{2g} mode and two peaks at 1,355 cm^{-1} (ascribed to edge planes and disordered structures) and 2,734 cm^{-1} (2D). In the Raman spectrum of the graphite oxide (Fig. 1b), the G band is broader and shifted to 1,581 cm^{-1}. The intensity of G band is reduced. On the other hand, the intensity of D band at 1,352 cm^{-1} increased significantly. The spectrum of the reduced graphite oxide (Fig. 1c) also contains both D and G bands (1,359 cm^{-1} and 1,588 cm^{-1}, respectively), however, the intensity of both peaks decreased. The ratio of the intensities (I_G/I_D) changed from 7.31 for the graphite to 0.51 for the graphite oxide (GO) and finally to 0.46 for the reduced material (RGO). These data indicate that chemical oxidation and thermal reduction cause distinct decrease of the size of the in-plane sp^2 domains and increase the degree of disorder in the prepared graphene-like material [26–30].

Scanning electron microscope (SEM) was used to characterize the structure of material before and after modification. Fig. 2a shows the image of the original graphite powder before the oxidation. The shape of individual particles, consisting of planes resembling a rose-like flower, is relatively regular. Fig. 2b present the graphite oxide reduced in the helium atmosphere (RGO-1). Special treatment of the material resulted in morphological changes manifested by irregular and disordered shape. It can be seen that material is composed of randomly aggregated, thin and wrinkled sheets, loosely coupled with each other. During galvanostatic charging/discharging process open spaces were filled with electrolyte decomposition products, resulting in the creation of a thin film on the material surface (Fig. 2c). Such a remarkable coating is the result of a high surface irregularities.

Fig. 3 shows the dependence of the discharge capacity (lithium insertion) vs. number of cycles for the RGO-1 and RGO-2 materials. In both cases, the capacity decreases rapidly during the first 10 cycles, then stabilizes during the next 15 cycles, remaining at the same level for the next 45 cycles. The main difference between these two materials was the value of the final capacity. The graphite oxide reduced in the presence of hydrogen reached the capacity of about 440 mAh g^{-1} after 70 cycles, almost 100 mAh g^{-1} less than that characteristic of the material obtained from GO reduced in the helium atmosphere (550 mA g^{-1}). Both materials were tested in the ionic liquid containing 20 wt.% VC as an SEI forming additive. The amount of VC which is added to the electrolytes based on ionic liquids is usually between 5 and 10 wt.%, depending on the type of the electrode material or the type of ionic liquid selected to examination [31–34]. However, due to the high irregularity of the material surface and the presence of numerous defects, causing a significant losses of capacity during the first lithium insertion (SEI formation), the content of VC in the electrolyte was increased to 20 wt.%. Cyclic performance of cells containing RGO-1 as a function of VC % in the electrolyte is shown in Fig. 3 (inset). As it can be seen, cell operating in Py13TFSI 0.7 M LiTFSI with 20 wt.% VC gives a higher value of capacity during first 30 cycles. In this case, the increase of VC amount resulted in well-developed SEI, improving the cell efficiency.

Charge and discharge curves for 1st and 2nd cycle are presented in Fig. 4. During the first insertion of lithium between the layers of the RGO-1 material the creation of protective SEI took place. The high capacity value of the first discharging process might be attributed to covering a number of defects on the surface and might be related with irreversible lithium storage. Retention of lithium within the structure of the material and lithium reactions with oxygen-containing functional groups (residues of the process of

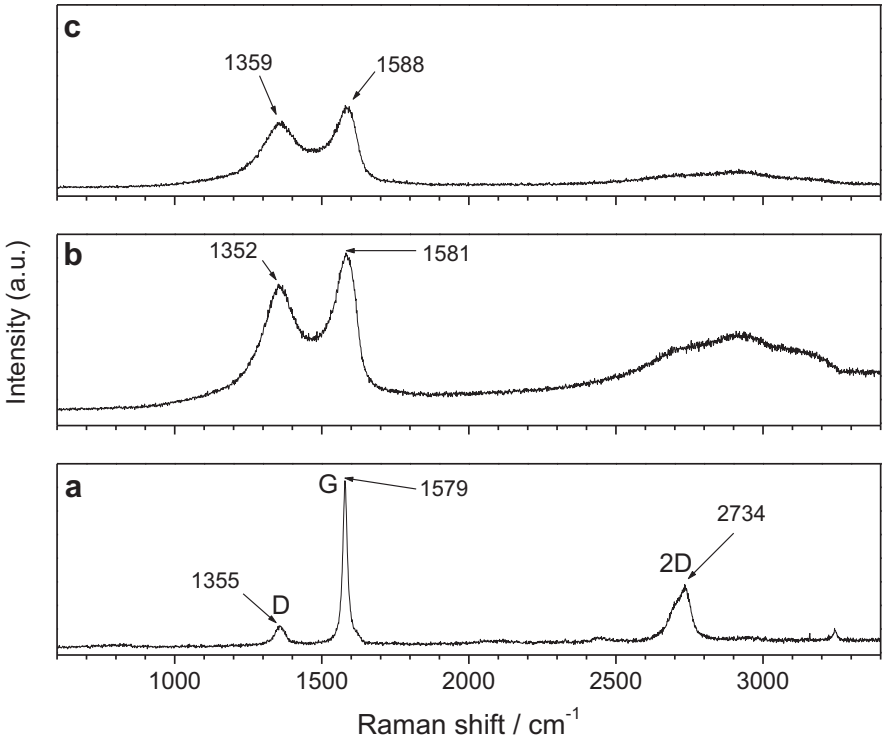

Fig. 1. Raman spectra of a) graphite b) graphite oxide c) reduced graphite oxide (RGO-1).

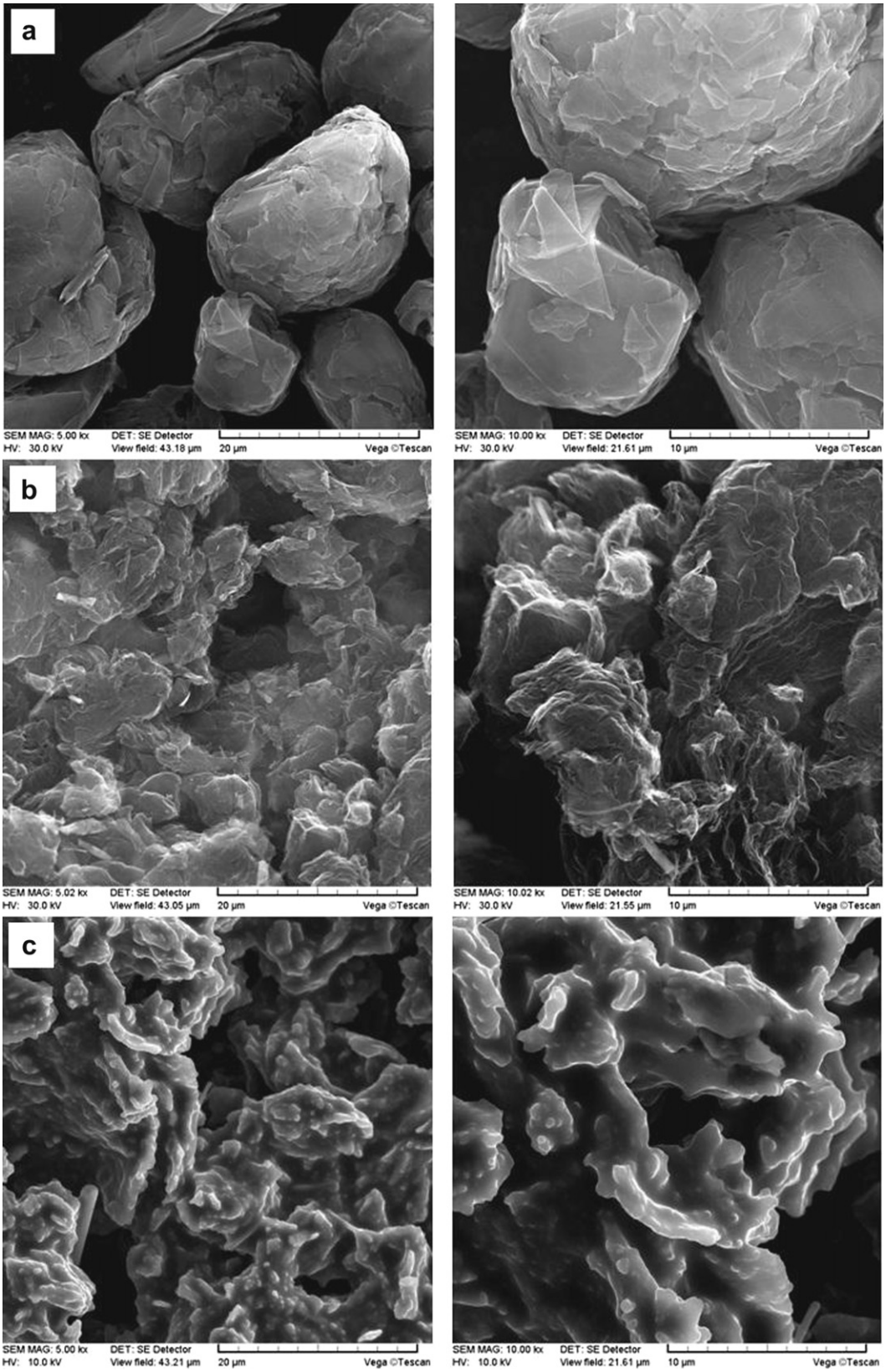

Fig. 2. SEM images of a) natural graphite powder b) RGO-1 c) RGO-1 electrode after galvanostatic charging/discharging.

oxidation and reduction) present on the material surface results in a capacity loss during 70 cycles to the value of 550 mA g^{-1} (stable during ca. 45 cycles), which is about 74% of the theoretical capacity. The coulombic efficiency of the first cycle was about 41%, which is related with SEI formation. However, the second-cycle efficiency was already twice higher (ca. 85%) and after the third cycle was stable at ca. 97%. All subsequent loss of the stored charge after the first cycle may be related to structural changes such as changing the

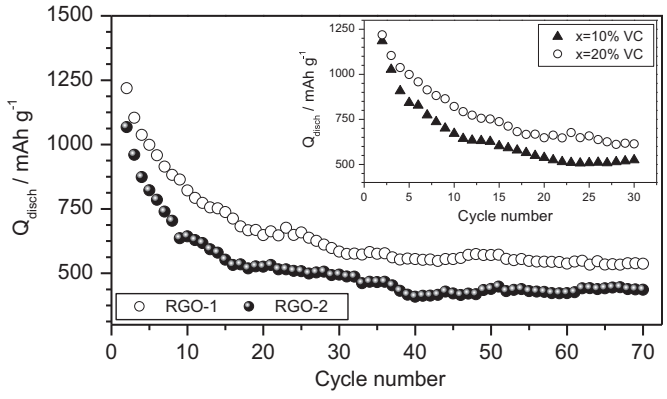

Fig. 3. Discharge capacity (lithium storage) of RGO in Py13TFSI 0.7 M LiTFSI + 20 wt.% VC and cyclic performance of cells containing RGO-1 as a function of VC % in the electrolyte (inset).

material arrangement, shifting layers or changing the distance between them. The shape of the curves in Fig. 4 does not represent a typical *plateau* indicating the process of lithium intercalation/deintercalation, characteristic for the electrode materials (especially graphite anode) used in lithium-ion batteries. The absence of such a *plateau* suggests electrochemically and geometrically unrepeatable location of Li^+ [35,36]. This may indicate that the process of lithium storage occurs in a different way in comparison to that characteristic of the graphite electrode. In addition, the process of storage and release of lithium ions does not proceed at the same potential range. The reaction of lithium with the active surface during the discharge processes (lithium storage) occurs at low voltages. However, the de-insertion of Li takes place at high voltages, because of the relatively strong interaction between the Li atoms and the surface rich in defects [37]. The mechanism of lithium storage may explain cyclic voltammetry diagram (Fig. 4, inset). The first reduction process is characterized by two fine peaks around 1.4 V and 0.9 V, probably corresponding to the formation of SEI on the surface of the anode. These peaks disappear during subsequent cycles, which can be attributed to the dense layer formation, separating the electrode from the electrolyte. The next stage of lithium insertion occurs at potentials below 0.5 V, giving a peak close to the residual value of 0.005 V. Difference between the CV curve of the first cycle and the other two cycles indicates that the irreversible capacity loss occurs predominantly in the first cycle [36]. In addition, it can be seen from the cyclic voltammetry, the region between 3 V and 1 V, which is close to the shape of a typical

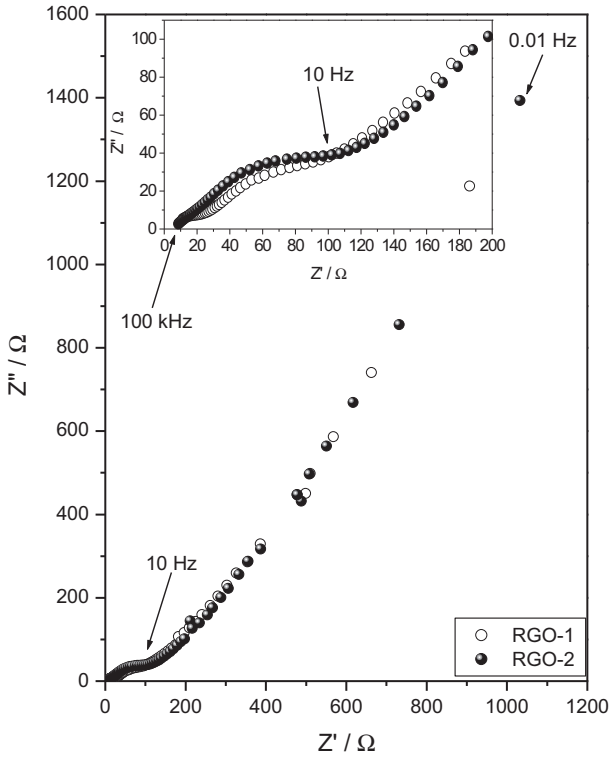

Fig. 5. Nyquist plots after 70 cycles of galvanostatic charging/discharging in Py13TFSI 0.7 M LiTFSI + 20 wt.% VC.

CV curve for electrochemical capacitors. It might be explained by the fact that the charge can be stored by the faradic reaction occurring on the surface or edges of the planes [21,38]. This phenomenon may be attributed to the properties of capacitive materials [39]. Some authors also suggest that lithium ions are electrochemically adsorbed on both sides of individual planes arranged in a random manner [21,40].

Fig. 5 shows the impedance curves of cells after 70 cycles of galvanostatic charge/discharge cycles. Both types of the electrode (RGO-1 and RGO-2) were in the delithiated state. Nyquist plot shows a fragment of semi-circles at high frequencies (100 kHz–10 Hz) with some slope in the region of low frequencies (10–0.01 Hz). Distorted semi-circles at high frequencies resulting from the superposition of several time constants are electrochemical response of the electrode processes such as the

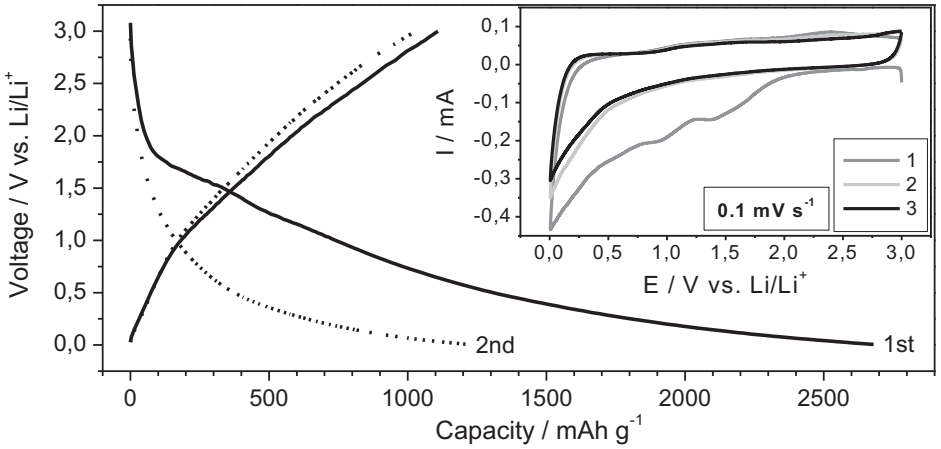

Fig. 4. Charge and discharge curves of RGO-1 in Py13TFSI 0.7 M LiTFSI + 20 wt.% VC and cyclic voltammetry (inset).

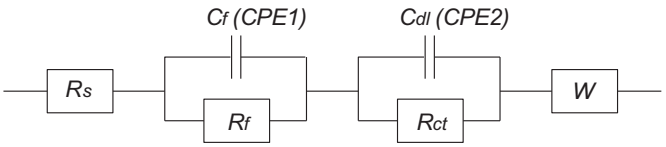

Fig. 6. Equivalent circuit representing electrolyte/electrode system.

migration of ions through the passivation layer (SEI), charge transfer resistance and the resistance of the electrolyte in the pores of the SEI. The straight line at low frequencies is responsible for the diffusion processes in the electrode active mass. It is worth noting that for two separate circuits, impedance spectra are almost the same. Impedance plots were analyzed by fitting to the equivalent circuit, shown in Fig. 6. In both cases the resistance of the electrolyte (R_s) was about 7 Ω, while the other values were different. For the cell with an electrode composed of RGO-1 material $R_f = 20$ Ω and $R_{ct} = 114$ Ω. The system contains material RGO-2 revealed slightly higher values of resistance, namely, $R_f = 29$ Ω and $R_{ct} = 134$ Ω.

4. Conclusions

1. This work is intended to show that the graphene-like material can be considerably good electrode material working with ionic liquid as electrolyte; these materials reveal comparable results with conventional electrolytes.
2. Obtained results showed that lithium storage process occurs reversibly with good cycling stability. Due to the structure of the material, creation of the SEI during the first lithiation process is associated with a large capacity loss.
3. Better performance (higher capacity) were obtained for the reduced graphite oxide in the presence of helium (RGO-1) rather than the material reduced in the presence of hydrogen (RGO-2).

Acknowledgement

The support of Polish Ministry of Science and Higher Education, grant No. IC-31 242/12 DS-BP is gratefully acknowledged.

References

[1] B. Scrosati, J. Garche, J. Power Sources 195 (2010) 2419–2430.
[2] M. Armand, J.M. Tarascon, Nature 451 (2008) 652–657.
[3] B. Scrosati, J. Hassoun, Y.K. Sun, Energy Environ. Sci. 4 (2011) 3287–3295.
[4] P.G. Bruce, B. Scrosati, J.M. Tarascon, Angew. Chem. Int. Ed. 47 (2008) 2930–2946.
[5] H. Li, Z. Wang, L. Chen, X. Huang, Adv. Mater. 21 (2009) 4593–4607.
[6] M. Armand, F. Endres, D.R. MacFarlane, H. Ohno, B. Scrosati, Nat. Mater. 8 (2009) 621–629.
[7] S.J. Wang, Y. Geng, Q. Zheng, J.-K. Kim, Carbon 48 (2010) 1815–1823.
[8] S. Yang, X. Feng, L. Wang, K. Tang, J. Maier, K. Müllen, Angew. Chem. Int. Ed. 49 (2010) 4795–4799.
[9] S.-M. Paek, E.J. Yoo, I. Honma, Nano Lett. 9 (1) (2009) 72–75.
[10] T. Wei, G. Luo, Z. Fan, Ch Zheng, J. Yan, Ch Yao, W. Li, Ch Zhang, Carbon 47 (2009) 2290–2299.
[11] H.-M. Ju, S.H. Huh, S.-H. Choi, H.-L. Lee, Mater. Lett. 64 (2010) 357–360.
[12] Ch Zhu, S. Guo, Y. Fang, S. Dong, ACS Nano 4 (4) (2010) 2429–2437.
[13] O. Akhavan, Carbon 48 (2010) 509–519.
[14] H.-L. Guo, X.-F. Wang, Q.-Y. Qian, F.-B. Wang, X.-H. Xia, ACS Nano 3 (9) (2009) 2653–2659.
[15] N. Liu, F. Luo, H. Wu, Y. Liu, Ch Zhang, J. Chen, Adv. Funct. Mater. 18 (2008) 1518–1525.
[16] M.D. Stoller, S. Park, Y. Zhu, J. An, R.S. Ruoff, Nano Lett. 8 (10) (2008) 3498–3502.
[17] J. Yan, T. Wei, B. Shao, F. Ma, Z. Fan, M. Zhang, Ch Zhen, Y. Shang, W. Qian, F. Wei, Carbon 48 (2010) 1731–1737.
[18] G. Srinivas, Y. Zhu, R. Piner, N. Skipper, M. Ellerby, R. Ruoff, Carbon 48 (2010) 630–635.
[19] H. Xiang, K. Zhang, G. Ji, J.Y. Lee, Ch Zou, X. Chen, J. Wu, Carbon 49 (2011) 1787–1796.
[20] D. Pan, S. Wang, B. Zhao, M. Wu, H. Zhang, Y. Wang, Z. Jiao, Chem. Mater. 21 (2009) 3136–3142.
[21] E.J. Yoo, J. Kim, E. Hosono, H.-S. Zhou, T. Kudo, I. Honma, Nano Lett. 8 (8) (2008) 2277–2282.
[22] G. Wang, X. Shen, J. Yao, J. Park, Carbon 47 (2009) 2049–2053.
[23] P. Guo, H. Song, X. Chen, Electrochem. Commun. 11 (2009) 1320–1324.
[24] W.S. Hummers, R.E. Offeman, J. Am. Chem. Soc. 80 (1958) 1339.
[25] A. Lewandowski, A. Swiderska-Mocek, J. Power Sources 171 (2007) 938–943.
[26] A.C. Ferrari, Solid State Commun. 143 (2007) 47–57.
[27] L. Wan, Z. Ren, H. Wang, G. Wang, X. Tong, S. Gao, J. Bai, Diamond Relat. Mater. 20 (2011) 756–761.
[28] P. Lian, X. Zhu, S. Liang, Z. Li, W. Yang, H. Wang, Electrochim. Acta 55 (2010) 3909–3914.
[29] S. Stankovich, D.A. Dikin, R.D. Piner, K.A. Kohlhaas, A. Kleinhammes, Y. Jia, Y. Wu, S.T. Nguyen, R.S. Ruoff, Carbon 45 (2007) 1558–1565.
[30] F. Tuinstra, J.L. Koenig, J. Chem. Phys. 53 (3) (1970) 1126–1130.
[31] T. Sato, T. Maruo, S. Marukane, K. Takagi, J. Power Sources 138 (2004) 253–261.
[32] M. Holzapfel, C. Jost, A. Prodi-Schwab, F. Krumeich, A. Würsig, H. Buqa, P. Novák, Carbon 43 (2005) 1488–1498.
[33] L. El Ouatani, R. Dedryvère, C. Siret, P. Biensan, D. Gonbeau, J. Electrochem. Soc. 156 (2009) A468–A477.
[34] X.G. Sun, S. Dai, Electrochim. Acta 55 (2010) 4618–4626.
[35] Z.H. Yang, H.Q. Wu, Mater. Lett. 50 (2001) 108–114.
[36] X. Li, D. Geng, Y. Zhang, X. Meng, R. Li, X. Sun, Electrochem. Commun. 13 (2011) 822–825.
[37] L.L. Tian, Q.C. Zhuang, J. Li, Y.L. Shi, J.P. Chen, F. Lu, S.G. Sun, Chin. Sci. Bull. 56 (2011) 3204–3212.
[38] R. Yazami, M. Deschamps, J. Power Sources 54 (1995) 411–415.
[39] T. Li, L. Gao, J. Solid State Electrochem. doi:10.1007/s10008-011-1384-x.
[40] J.S. Xue, J.R. Dahn, J. Electrochem. Soc. 142 (1995) 3668–3677.